Journal of Marine Research, 55, 453–481, 1997

Monitoring the upper southeastern Atlantic transports using altimeter data

by Silvia L. Garzoli[1,2], Gustavo J. Goñi[3], Arthur J. Mariano[3] and Donald B. Olson[3]

ABSTRACT

A large *in-situ* data set, collected in the southeastern Atlantic Ocean, is merged with the TOPEX/POSEIDON altimeter observations in order to verify the use of altimeter data in monitoring the transports of the Agulhas/Benguela system. Comparisons between altimeter observations and either moored current meters or inverted echo sounder measurements shows that the sea-surface elevation anomaly is significantly correlated with the thermocline depth and the surface dynamic height, respectively. Knowing the least-squares regression parameters, it is possible to calculate the transports by using geostrophy and either a two-layer or a continuously-stratified model. The transports obtained from fits of dynamic height to altimeter sea-surface height are similar to the ones calculated with the moored instruments. In the southern part of the area under analysis, around 35S, close to the Agulhas retroflection, the transports obtained from the two-layer model are overestimated. Across the Benguela Current, at 30S, transports are still overestimated but of the same order as the measured ones. In this part of the region, the two-layer model can be successfully used to calculate the total and barotropic transports of the Benguela Current. Analysis of the three years of geostrophic transport obtained from the altimeter data indicate that the mean Benguela Current transport does not change interannually more than 20%. However, the primary interannual variability derives from the source water that forms the Benguela Current.

I. Introduction

The oceanic circulation of the southeastern Atlantic is of particular interest not only because of its complexity but also because of its importance as a gateway for Indian-Atlantic Ocean exchange of mass, heat and salt. The interocean exchange takes place primarily through a process of eddy detachment and associated entrainment from the Agulhas retroflection. Large pulses of warm and salty water enter the Atlantic in the form of Agulhas eddies (e.g., Gordon, 1985; Lutjeharms and van Ballegoyen, 1988). The main instrument of entrainment of these waters into the Atlantic is the Benguela Current, the broad northward flow adjacent to southwestern Africa that forms the eastern limb of the

1. National Oceanic and Atmospheric Administration, Atlantic Oceanographic and Meteorological Laboratory, 4301 Rickenbacker Causeway, Miami, Florida, 33149, U.S.A.

2. On leave of absence from Lamont-Doherty Earth Observatory, Columbia University, Palisades, New York, 10964, U.S.A.

3. Rosenstiel School of Marine and Atmospheric Science, University of Miami, 4600 Rickenbacker Causeway, Miami, Florida, 33149, U.S.A.

South Atlantic subtropical gyre (Stramma and Peterson, 1990; Peterson and Stramma, 1991). At 30S, the entire Benguela Current is confined between the African coast and the Walvis Ridge located at 3E (Fig. 1).

During the years 1992 and 1993, a cooperative program between U.S. and South African scientists called Benguela Sources and Transports, BEST, took place in the southeastern Atlantic. The primary objectives of this program were to determine the sources of the Benguela Current and to measure its transport and variability (Garzoli *et al.,* 1995). As part of this program, an array of current meter moorings, CMM, and inverted echo sounders, IES, were deployed at the locations shown in Figure 1. The Benguela Current is assumed to have a strong barotropic component (e.g., Olson and Evans, 1986). Based on the work by Chiswell *et al.* (1986), who proved that a measure of both barotropic and baroclinic components of the transport could be obtained with a combination of IES and pressure, P, data, the IES deployed along 30S were equipped with pressure sensors, PIES, to quantify both modes.

In a first analysis of the BEST hydrographic and IES data, Garzoli and Gordon (1996) calculated the baroclinic transports of the upper kilometer of water associated with the Benguela/Agulhas system and the patterns of the general circulation. According to Garzoli and Gordon (1996), the mean transport of the Benguela Current during the BEST experiment is 13 Sv. Fifty percent of these 13 Sv is derived from the southwest and may be chiefly South Atlantic water; 25% from the Indian Ocean (Agulhas Water); and 25% from the east. This last source is mainly a blend of Agulhas water filaments that flow north along the African coast, and tropical Atlantic water that flows south in the form of the Benguela Coastal Current (Fig. 1). The baroclinic and barotropic transport carried by the Benguela Current into the South Atlantic was calculated by Garzoli *et al.* (1996) from all available data. One of the main results from this last work is that the Benguela Current has two main components: a stationary part that flows between the African coast and 8E, and a transient component that flows between 8E and the Walvis Ridge (3E). The baroclinic signal is dominant (75%) in the steady component. On the other hand, in the transient component associated with the passage of the Agulhas rings, the barotropic and baroclinic signals, are equally important (50% of the transport corresponds to each mode). The total annual mean northward transport was estimated to be of the order of 15 Sv. This transport undergoes significant seasonal changes, with an indication of interannual variability. However, due to the length of the available records (18 months of data), the characteristics of these interannual variations cannot be well described.

Goñi *et al.* (1996) showed that the GEOSAT altimeter sea-surface height anomaly data are a good proxy for the depth of the thermocline in the southwestern Atlantic. Values of the anomaly in sea-surface height, η', were correlated to the depth of the upper layer thickness anomaly, h'_1, in a two-layer model. A three-year time series of the transports of the Brazil and Malvinas Currents at their confluence were calculated using this model and the GEOSAT data.

In this study, the TOPEX/POSEIDON (T/P) data are analyzed together with the BEST

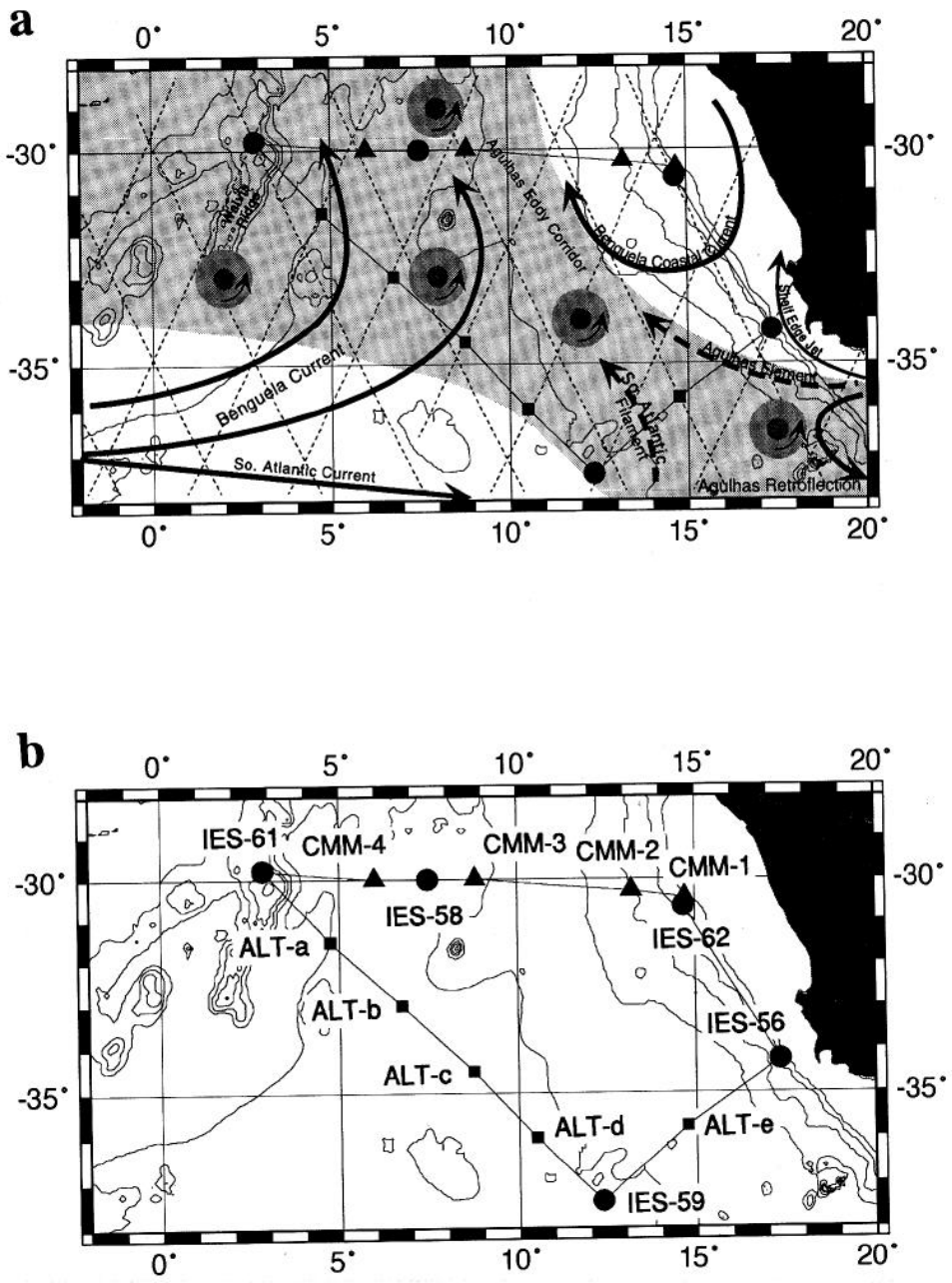

Figure 1. The region of study. Bathymetry is in intervals of 1000 m. (a) Schematic of the oceanic circulation. The TOPEX tracks are indicated by dotted lines. The location of the deployments by circles and triangles. Interpolation points are squares. The shaded area indicates the eddy corridor (big circles are rings) according to Garzoli *et al.* (1996). (b) Detail on the deployment sites, station names, and interpolation points (see text).

data in order to extrapolate the BEST results in time and space. The goals are improved estimates of seasonal and interannual transport variability through longer term monitoring from space. In anticipation of this analysis, the BEST PIES along 30S were deployed close or near T/P ground tracks to optimize the validation.

The *in-situ* and satellite data sets used in this study are detailed in Section 2. A relationship between the altimeter-derived sea-surface height anomaly, and the depth of the thermocline and the dynamic height derived from the inverted echo sounder records are calculated in Section 3. The series obtained through this procedure are analyzed using the methods from Garzoli and Gordon (1996) and Goñi *et al.* (1996) to obtain transports of the upper kilometer and the upper layer of the ocean, respectively. The characteristics of a three-year transport time series from October 1992 until September 1995 are discussed in Section 4.

2. The data

a. Satellite data. The T/P altimeter data are processed by applying corrections similar to those described in detail by Cheney *et al.* (1987), which include solid and ocean tides (Cartwright and Ray, 1990), wet and dry tropospheric, ionospheric, EM bias and inverse barometric corrections. The corrected heights are interpolated onto a 0.2 degree of longitude along-track grid. A mean or reference sea-surface height track is computed for each track using all data and a slightly modified collinear approach similar to that proposed by Chelton *et al.* (1990). This method estimates the mean sea height from the mean along-track slope of interpolated sea heights at fixed grid points in a process equivalent to integration, i.e., by reconstructing the curve from its mean slope value at each grid point. It should be noted that only the value of the anomaly, η', is calculated because the absolute sea-surface topography cannot be estimated accurately from the currently available geoid model.

Values of η' obtained by this procedure from different sites cannot be compared directly because the time mean sea-surface height changes spatially. However, at a fixed site changes in η' are the same as changes in sea height, η. This concept is used in the following sections when the same meaning is given to both variables, sea-surface height, and sea-surface height anomaly.

The IES locations were chosen to lie close to the T/P ground tracks to facilitate the comparison with altimeter data (Fig. 1). The comparison between T/P altimeter data and the IES data is done for the period October 1992, the beginning of the T/P mission, to September 1993, the last date of the available IES data set. However, problems with calibration of T/P attitude control degraded the quality of altimeter height observations through most of 1992 (Hayne *et al.*, 1994). Data collected during this period that will fall at more than two standard deviations in the regression analysis were not used in the correlations performed in Section 3.

In order to estimate the η' values as close as possible to the IES locations and to account for the mesoscale features present in the area, the objective analysis, OA, scheme described

in Mariano and Brown (1992) is used to interpolate η' onto a 0.2 degree latitude/longitude grid every five days. The following anisotropic and time-dependent correlation model,

$$C(dx, dy, dt) = C(1)[1 - (DX/C(4))^2 - (DY/C(5))^2] \cdot e^{-[(Dx/C(6))^2 + (DY/C(7))^2 + (dt/C(a))^2]} \quad (1)$$

$$DX = dx - C(2) \cdot dt \text{ and } DY = dy - C(3) \cdot dt, \quad (2)$$

was assumed (see Mariano and Brown, 1992). *dx*, *dy* and *dt* are the east-west, south-north, and temporal lags, respectively. The nine correlation parameters, in units of degrees longitude, latitude, and days, are a normalized error variance (C1) of 0.30; east-west and south-north phase speeds (C2, C3) of −0.04, 0.0, respectively; east-west and south-north zero-crossing scales (C4, C5) of 2.0, 2.0; spatial *e*-folding scales (C6, C7) of 1.4, 1.4; a temporal *e*-folding scale (C8) of 20 days; and a rotation angle (C9) of 0. Figure 1 shows the BEST deployment sites and the T/P ground tracks overlapped to a schematic of the circulation in the region according to Garzoli *et al.* (1996).

b. Oceanic data. An inverted echo sounder is a bottom-deployed instrument that measures the time that it takes for an acoustic signal emitted at the bottom to reflect at the surface and return back to the bottom. This time, called the travel time, is directly correlated to the depth of the thermocline and to the dynamic height in the North Atlantic, tropical Atlantic, and southwestern Atlantic (e.g., Watts and Rossby, 1977; Katz and Garzoli, 1982; Garzoli and Garraffo, 1989, respectively). In the southeastern Atlantic, Duncombe-Rae *et al.* (1996) used the BEST CTD data and historical data to obtain a significant correlation between changes in travel time, $\Delta\tau$, and changes in depth of the 10°C isotherm, Δh_{10},

$$\Delta h_{10} = -2.96(\pm 0.40)\, \Delta\tau \quad (3)$$

with a correlation coefficient $r^2 = 0.97$. This isotherm proved to be a good proxy for the depth of the thermocline or the depth of the upper layer in the region.

Relationship (3) was applied to the travel time series to obtain five time series of the anomaly variability for the duration of the experiment. Series of h_{10} were afterward obtained by adjusting the Δh_{10} series to the values of h_{10} measured with three CTD casts obtained at each IES deployment site during the three BEST cruises. The adjustment is done by minimizing the deviations of the IES records from the CTD casts (see Duncombe-Rae *et al.* (1996) for details in the procedure).

In addition to these five 10°C isotherm depth time series from the IES, four additional time series were obtained by Garzoli *et al.* (1996) from the CMM data collected during the BEST experiment. The depth of the 10°C isotherm, h_{10}, was determined through a linear interpolation of the temperature measurements collected with the two current meters deployed at the top of the mooring at approximately 210 and 512 m depth. In the event that the depth of the 10°C isotherm was deeper than 512 m, the depth of a higher isotherm (11° or 12°C) was determined. The time series of thermocline depth derived from these two data sets are shown in Figure 2. Accuracy of the linear interpolation of the moored temperature

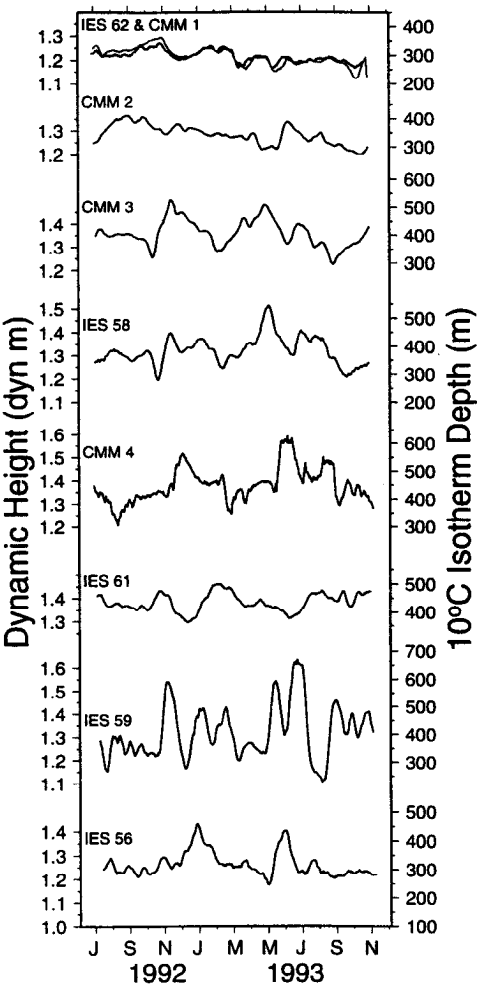

Figure 2. Series of the 10°C isotherm (right scale) and dynamic height (left scale) obtained from the five IES and four CMM data sets at the IES and CMM locations indicated in Figure 1.

sensors is tested by comparing the results obtained at CMM1 and PIES62. These two instruments were deployed 23.3 km apart from each other (Fig. 1). This is a small distance for the scales of the motions involved and, therefore, the main variability of the series should compare. The series obtained with both methods are very similar (Fig. 2, top panel), and the small differences observed can be attributed to small-scale spatial variability.

Garzoli *et al.* (1996) converted the nine series of h_{10} to time series of anomaly in dynamic height by using the following relationship obtained between anomalies in surface dynamic height (ΔD) (assuming a level of no motion at 1000 m), and anomalies in depth of the 10°C isotherm (Δh_{10})

$$\Delta D(\text{dyn m}) = 9.48 \times 10^{-4}\, \Delta h_{10}(\text{m}). \tag{4}$$

Values of ΔD were afterward adjusted to dynamic height at the surface, reference 1000 m, using the CTD casts obtained at the location of the deployments during the three BEST cruises. As this is only a problem of scaling, the series obtained through this procedure are the same as those obtained for the depth of the 10°C isotherm. The time series of D are shown in Figure 2 where the left-hand side scale corresponds to dynamic height of the surface reference 1000 m.

The variability of the 10°C isotherm time series measured close to the continental shelf (Fig. 2, IES 62, CMM1) and near the Walvis Ridge (Fig. 2, IES 61) is smaller than the variability near the center of the basin which is dominated by the eddy field and the passage of rings. Duncombe-Rae *et al.* (1996) showed that Agulhas eddies can be identified as large depressions in the depth of the 10°C isotherm series that range between 200 and 500 m. Depressions of these magnitudes are not observed close to the African coast (Fig. 2) but start to become significant at 8°50′E (location of CMM 3). They are also significant at the site of IES 59, a location that has been identified as characteristic of detecting the passage of large eddies (Garzoli and Gordon, 1996). Garzoli *et al.* (1996) determined that the speed of propagation of these rings ranges between 7 km/day to 13 km/day, and that these eddies lose energy and their velocity decreases in their motion across the Atlantic.

3. Transports

Two different methods are used to estimate transports from the data sets described above. Method 1 is based on altimeter-derived upper layer thickness (defined here from the sea surface to the depth of the thermocline). The second method is based on the relationship (4) between the sea-surface height anomaly and the dynamic height of the sea surface to a reference level of 1000 m.

a. Upper layer thickness and transports from a two-layer model. The model used to obtain the upper layer transports is described in detail by Goñi *et al.* (1996). In this model (see Fig. 3) the vertical structure of the ocean is described by two layers with a discontinuity at the main thermocline, represented in this region by the 10°C isotherm (Olson and Evans, 1986; Duncombe-Rae *et al.,* 1996). The thermocline deviations can be related to pressure associated with the baroclinic structure of the circulation through reduced gravity, g',

$$g' = g(\rho_2 - \rho_1)/\rho_2 \tag{5}$$

where g is gravity, and ρ_1 and ρ_2 are the densities of the upper and lower layers, respectively. This model also assumes that the lower layer is in motion and tied to a vertical constant barotropic component of the horizontal pressure gradient in both layers. Following Goñi *et al.* (1996), the sea-surface height, η, and sea-surface height anomaly, η', can be written as a function of both baroclinic and barotropic components:

$$\eta(t) = \epsilon\, h_1(t) + B(t) \tag{6}$$

$$\eta'(t) = \epsilon\, h_1'(t) + B'(t), \tag{7}$$

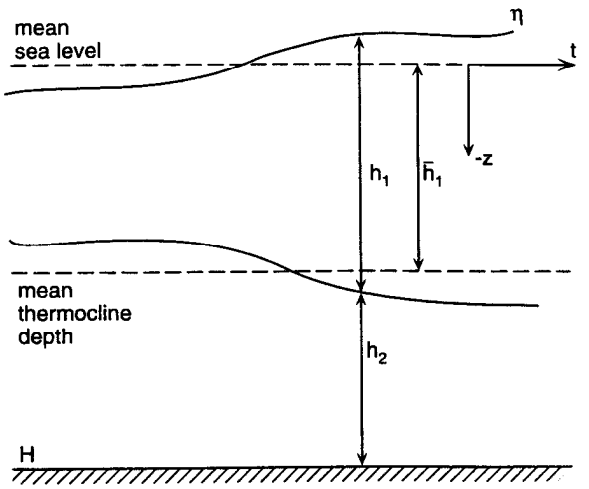

Figure 3. Schematic of the two-layer model after Goñi *et al.* (1996). h_1 and h_2 are the upper and lower layer thicknesses, respectively. η' is the sea height anomaly and H is the ocean depth.

where $\epsilon = \rho_2/(\rho_2 - \rho_1)$, $h_1(t)$ is the upper layer thickness, $h'_1(t)$ is the upper layer thickness anomaly, $B(t)$ is the barotropic component of the sea-surface height,

$$B(t) = \rho_1/\rho_2\, h_1(t) + h_2(t) - H, \tag{8}$$

$B'(t)$ is the barotropic component of the sea-surface height anomaly, and H is the ocean depth. The thickness of the upper layer can be written as

$$h_1(t) = \overline{h_1} + \frac{1}{\epsilon}[\eta'(t) + B'(t)], \tag{9}$$

where $\overline{h_1}$ is the mean upper layer thickness.

The geostrophic velocity for layers 1 and 2, $\mathbf{v}_1$ and $\mathbf{v}_2$, respectively, is given by

$$\mathbf{v}_1 = f^{-1}\,\hat{k} \times [g'\nabla h_1(x, t) + g\nabla B(x, t)], \tag{10}$$

and

$$\mathbf{v}_2 = f^{-1}\,\hat{k} \times \nabla B(x, t), \tag{11}$$

where f is the Coriolis parameter.

The baroclinic transport is computed by assuming that the bottom layer is at rest and that every change in the thickness of the upper layer corresponds to a change in sea-surface height. Under these assumptions, the baroclinic transport in the upper layer $S_{cl}(t)$ is

$$S_{cl}(t) = \frac{g'}{2f}\Delta h_1^2(t), \tag{12}$$

Table 1. Results of a linear regression between anomalies of the sea-surface height and depth of the upper layer (5). ϵ is the slope of the regression.

Site	ϵ	Error in ϵ	%	r	r^2
CMM1	8.23E-04	1.71E-04	21%	0.68	0.46
CMM2	*8.01E-04*	*2.00E-04*	*25%*	*0.59*	*0.35*
CMM3	1.10E-03	1.00E-04	9%	0.84	0.70
CMM4	9.54E-04	1.35E-04	14%	0.78	0.60
IES 56	1.88E-03	2.41E-04	13%	0.84	0.70
IES 58	4.82E-04	9.10E-05	19%	0.70	0.50
IES 59	1.83E-03	1.75E-04	10%	0.88	0.78
IES 61	1.32E-03	1.33E-04	10%	0.89	0.80
IES 62	1.49E-03	2.62E-04	18%	0.71	0.50
Mean ϵ = 0.00119			g' = 0.0116 m/sec^2		
Statistics of all points from nine series:					
ϵ =	0.00126	±0.000074	g' =	0.0123 m/sec^2	r^2 = 0.47
Statistics of all points from seven series along 30S:					
ϵ =	0.00081	±0.000070	g' =	0.0079 m/sec^2	r^2 = 0.34
Statistics of all points from 2 series in the south (56 and 59):					
ϵ =	0.0021	±0.00035	g' =	0.0206 m/sec^2	r^2 = 0.50

where $\Delta h_1(t)$ is the time series for the upper layer thickness difference between the locations where the transport is being computed. The upper layer barotropic transport is obtained from

$$S_{tr}(t) = \frac{\overline{H}g}{f} \Delta B(t), \tag{13}$$

where $\overline{H}$ is the mean ocean depth between sites a and b, and ΔB is the barotropic sea-height difference between the sites (see Goñi *et al.* (1996) for the derivation of (12) and (13)).

b. Depth of the thermocline from the altimeter data. The major analysis assumption is that a significant correlation exists between the sea-surface height anomaly, $\eta'(t)$, and the anomaly of the thickness of the upper layer, $h'_1(t)$.

Table 1 shows the results of a linear regression of the sea-surface height anomaly as a function of the depth of the upper layer thickness anomaly (7). The value of the slope in the regression is the parameter ϵ. The upper portion of Table 1 lists the estimates of ϵ at each IES and CMM site along with the error of the estimate, the error percentage, and the correlation coefficient. The estimated values of ϵ, which range from 0.5×10^{-3} to 1.88×10^{-3}, are also shown at each location in Figure 4. With the exception of sites CMM1 and CMM 2, the relative errors are smaller than 20%. The highest relative errors are observed at sites IES 56 and 59, which are the southernmost in the array. The mean value of ϵ is 1.19×10^{-3} which yields a value of $g' = 0.0116$ m/sec^2.

Separate regressions are given in the lower part of the Table 1 for different groupings of instruments. When the analysis is performed for all nine series, the value of g' obtained is

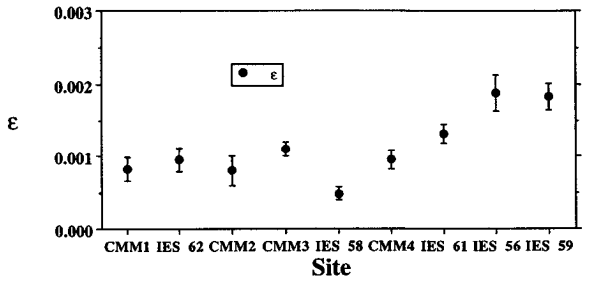

Figure 4. Estimated values of ϵ and its error as a function of the location site.

0.0126 m/sec^2, similar to the mean value of the individual estimates. Note that this value is only equal to the mean of the individual regressions if the samples contain the same number of data points and this is not the case here. For the seven series along 30S, $g' =$ 0.008 m/sec^2 and for the two stations in the southern part of the analyzed region, g' is 0.021 m/sec^2.

In order to verify these results, the CTD data collected during the three BEST cruises are used to obtain the value of g' for the area which are given in Table 2. As an example, results from the data collected during May 1994 (BEST 2) are shown graphically in Figure 5. The mean value of g' for the three BEST cruises is 0.011 m/sec^2, in agreement with those obtained from the correlation between the depth of the 10°C isotherm obtained from the IES data and the sea-surface height measured with the altimeter.

On the basis of this good agreement, similar regressions were obtained to determine the depth of the upper layer thickness anomaly, h'_1, from the altimeter-derived sea-surface height anomaly, η'

$$h'_1(t) = A\eta'(t) + C. \tag{14}$$

The computed regression coefficients from (14), A and C, are given in Table 3. The relative errors of the thickness anomaly estimates are all lower than 20%. The time series of the estimated h'_1 obtained at each mooring site through these regressions are shown in Figure 6. The empty circles show the IES and CMM-derived h'_1 values, while the solid circles show the altimeter-derived h'_1 values using (14). The right-hand side panel shows the linear fits between h'_1 and η', where the slope is given by ϵ.

Table 2. Values of g' calculated from the CTD data collected during the three BEST cruises.

			g'(m/sec^2)		
Cruise	Dates	Number of stations	Minimum	Maximum	Mean
BEST 1	6/17 to 7/4/92	35	0.001	0.015	0.010
BEST 2	5/7 to 6/2/93	74	0.008	0.017	0.012
BEST 3	10/25 to 11/9/93	35	0.006	0.014	0.011
				Mean	0.011

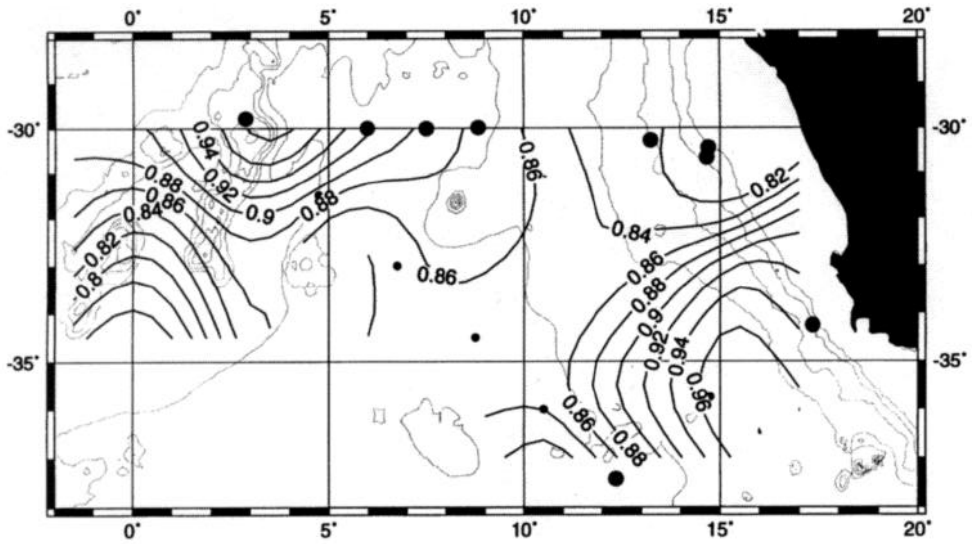

Figure 5. Map of distribution of g', the reduced gravity value, obtained from the BEST 2 CTD data.

c. Upper layer baroclinic transports. The baroclinic transports between station pairs above the thermocline are obtained using the formulation given previously from the h_{10} series and the values of ϵ calculated at each site. For example, the value of the transport between stations 56 and 59 is obtained using the mean value of ϵ at stations 56 and station 59. The transport computations are done using either the depth of the thermocline inferred from the moored data or the depth of altimeter-derived upper layer thickness.

The error in the transport computation is due primarily to the error incurred in estimating the upper layer thickness anomaly. According to Table 3, these errors range from ± 19 to ± 50 m.

Table 3. Results of the regression between anomalies in depth of the upper layer and sea-surface height (12). Amplitude is the amplitude of the oscillations observed at each site and used to determine the relative errors.

Site	A	C	r	r^2	r^2 RMS (m)	Amplitude	Relative error
CMM1	558.58	−4.56	0.68	0.46	19.71	103.30	19%
CMM2	418.07	−6.56	0.58	0.34	23.42	128.00	18%
CMM3	567.61	3.52	0.85	0.72	28.40	209.00	14%
CMM4	631.64	8.64	0.78	0.60	32.69	226.99	14%
IES 56	371.11	8.36	0.84	0.70	27.90	186.50	15%
IES 58	1,030.13	11.03	0.71	0.50	49.81	263.00	19%
IES 59	426.74	5.38	0.88	0.78	44.12	370.81	12%
IES 61	580.80	1.47	0.88	0.77	18.88	130.00	15%
IES 62	336.94	−4.80	0.71	0.50	14.04	103.00	14%
Mean	546.85	2.50					

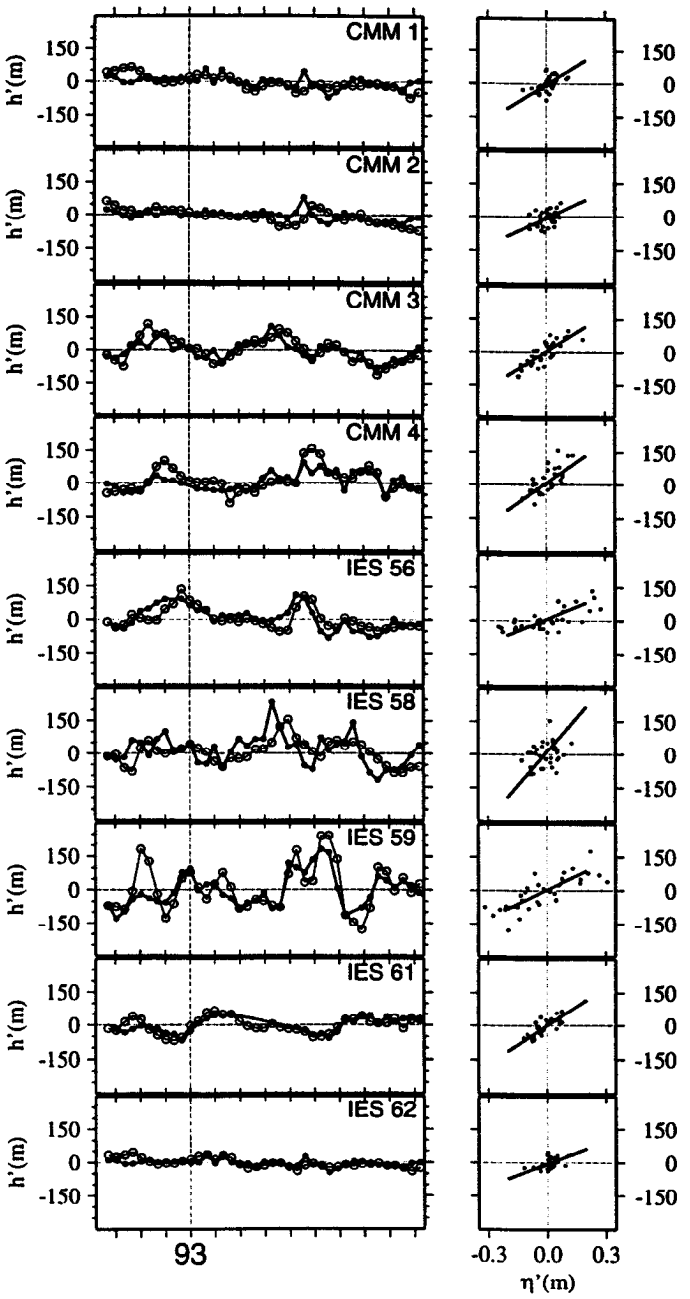

Figure 6. Values of h'_1 as a function of time measured from the moored instruments (empty circles) and derived from the regressions (black circles) shown in the right panel at the locations indicated in Figure 1.

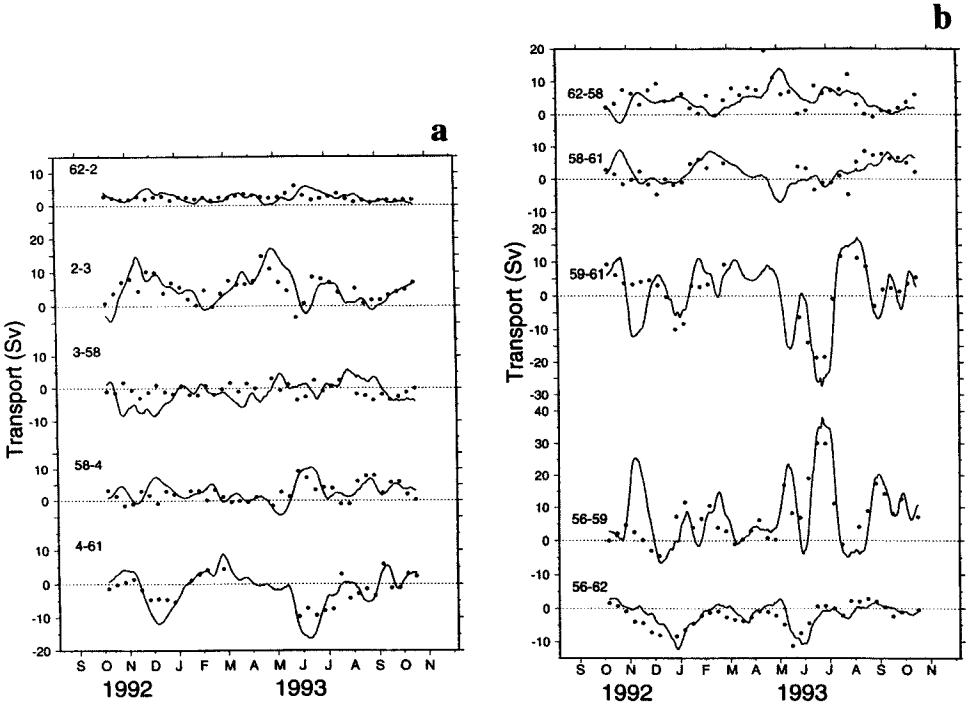

Figure 7. Transports of the upper layer obtained from the two-layer model. The solid line corresponds to transports obtained from the series of depth of the 10°C isotherm, h_{10}, measured with the moored instruments. Dots are the same transports derived from the altimeter-derived h'_1. Values of ϵ are variable and determined at each site: (a) for stations along 30S; (b) for the analyzed box.

The upper-layer baroclinic transports are calculated along 30S and in a closed box formed by the locations of IES 62, 58, 61, 59, and 56, using data only from the IES moorings to compare with the results of Garzoli and Gordon (1996). The time series for these transports along 30S are shown in Figure 7a, where the solid lines and circles correspond to the IES-derived and altimeter-derived transports, respectively. Similarly, Figure 7b shows the time series for the closed box. The statistics of these series are given in Table 4.

In general, the agreement between transport estimates obtained from the moored data and from the altimeter measurements is good (Figs. 7a,b). Despite the short time scale differences expected (moorings deployed at 23 km apart show differences in the data collected due to the high variability of the area), the mean features and trends observed with the moored instrumentation are also exhibited by the altimeter-derived transports (Fig. 7). This is true for most of the comparison period with the exception of a period of time around the end of 1992. At that time, the beginning of the T/P data, there is a discrepancy between the two products. This could be due to the fact that the altimeter data

Table 4. Comparison between the statistics of the transport files obtained from the moored data and altimeter data for the overlapping period of observations.

Along 30S	Station pairs	Minimum	Maximum	Mean	Delta mean
Altimeter	62 and 2	0	6	2.2	
Moorings	*62 and 2*	*0.1*	*6.7*	*2.8*	*−0.6*
Altimeter	2 and 3	−3.4	14.7	5	
Moorings	*2 and 3*	*−3*	*16.8*	*5.1*	*−0.1*
Altimeter	3 and 58	−3.7	10.5	−0.5	
Moorings	*3 and 58*	*−8.3*	*4.4*	*−1.8*	*1.3*
Altimeter	58 and 4	−7.8	9.2	2.5	
Moorings	*58 and 4*	*−4.5*	*10.5*	*2.3*	*0.2*
Altimeter	4 and 61	−9.8	6	−1.6	
Moorings	*4 and 61*	*−16.1*	*8.7*	*−1.8*	*0.2*
Closed box	Station pairs	Minimum	Maximum	Mean	Delta mean
Altimeter	56 and 59	−4.4	30.1	7	
Moorings	*56 and 59*	*−6.2*	*35.6*	*8.8*	*−1.8*
Altimeter	56 and 62	−11.3	2.8	−2.3	
Moorings	*56 and 62*	*−11.9*	*2.7*	*−1.7*	*−0.6*
Altimeter	62 and 58	−0.7	19.5	5.2	
Moorings	*62 and 58*	*−2*	*13.9*	*4.2*	*1*
Altimeter	59 and 61	−18.6	11.7	0.9	
Moorings	*59 and 61*	*−25.4*	*17.3*	*0.1*	*0.8*
Altimeter	58 and 61	−4.6	8.7	2.3	
Moorings	*58 and 61*	*−1.9*	*8.3*	*3*	*−0.7*

during 1992 experienced problems with the attitude and tracking of the satellite (Hayne *et al.*, 1994).

The annual mean of the transports (Table 4) from the different methods agree to within 1.8 Sv. Along 30S, the total baroclinic transport of the upper layer across the section is 7.6 Sv in the altimeter estimate and *6.6* Sv when computed from the moored data. If we designate the values of the transports from the moored data by italics in parentheses, Table 4 shows that 1 *(2)* Sv of South Atlantic water enters the box through stations 61 and 59; 7 *(8.8)* Sv of Indian Ocean waters are entrained by the Benguela retroflection between stations 59 and 56; and 2.3 *(1.7)* Sv of tropical are entrained by the Benguela retroflection between stations 59 and 56; and 2.3 *(1.7)* Sv of tropical water is coming from the east and a blend of Agulhas filaments and tropical waters flowing south along the African coast entering the box between stations 56 and 62.

d. Transports from dynamic height series. In the previous section the transports for the upper layer were estimated on the assumption that a two-layer model is representative of the vertical structure of the ocean. In this section, the altimeter data are scaled to dynamic height using (4) for the purpose of comparing the results with those previously obtained in the area. Since there is only a difference in scale between the dynamic height series and the

depth of the 10°C isotherm series, the statistics of the correlations obtained between sea-surface height and dynamic height are the same as those obtained between η' and Δh_{10} and, therefore, the details of its computation are not shown in this paper.

The geostrophic meridional velocities, V_g, are obtained from the dynamic height values by using the relationship

$$V_g = \frac{g}{f}\frac{\delta D}{\Delta x} \tag{15}$$

where δD is the difference in dynamic height between two stations separated by a distance Δx, g is the gravity, and f the Coriolis parameter.

The velocities obtained using (15) correspond to the baroclinic component of the geostrophic motion. Geostrophic transports are then calculated using the approximation that the geostrophic velocity decreases proportionally with depth. Under this assumption, the geostrophic transports, T_r, are calculated through the relationship

$$T_r = kV_g \Delta x \Delta z, \tag{16}$$

where k is an empirically-determined constant (Garzoli and Gordon, 1996), and Δz is the depth of the reference level. Garzoli and Gordon (1996) demonstrated the validity of (16) by analyzing the vertical profiles of geostrophic velocity and determining the error committed in assuming a linear decrease of V_g with depth. The error was estimated to be ± 1 Sv and the transport values calculated through this procedure are interpreted as estimates of the lower limits.

During the BEST experiment the instruments deployed along 30S were equipped with a pressure sensor. These sensors allowed for the calculation of the variable part of the total geostrophic velocity between station pairs by using the formulation (Garzoli *et al.*, 1996)

$$V'^{\,\text{Total}}_{g} = \frac{g}{f}\frac{\Delta D'}{\Delta x} + \frac{1}{\rho_0 f}\frac{\Delta P'}{\Delta x} \tag{17}$$

where ρ_0 is the standard density and $\Delta P'$ is the difference between pressure anomaly between stations separated by a distance Δx.

The first term on the right-hand side of (17) corresponds to the relative part of the baroclinic component of the total velocity, which can be obtained from the IES records of travel time as explained above. The second term on the right-hand side is the relative part of the barotropic component of the total velocity, and can be calculated by measuring the difference in pressure between two stations separated by a distance Δx. The total absolute geostrophic velocity is afterward obtained using CTD, ADCP, and current meter data (Garzoli *et al.*, 1996) to determine the mean velocity that is added to the relative velocity.

A comparison between the geostrophic transport series obtained by Garzoli *et al.* (1996) and the ones derived in this paper from the altimeter data are shown in Figure 8 and Table 5. The agreement is, in general, good and within the estimated error bounds. These

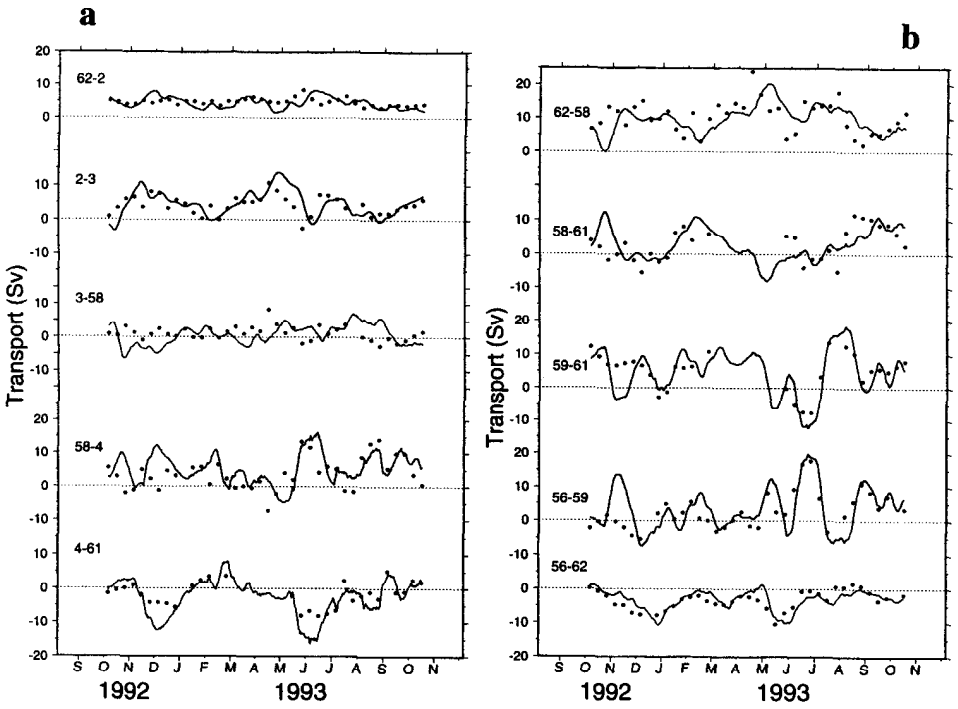

Figure 8. Comparison between the transport series (from the surface to 1000 m) obtained by Garzoli *et al.* (1996) and the ones calculated applying the same method to the dynamic height series derived from the altimeter data: (a) for stations along 30S; (b) for the analyzed box.

calculations are used below to compare with the baroclinic transports obtained with the two-layer model.

e. Transports from the two-layer model versus transport from dynamic height. A comparison between the results obtained by the two different methods using altimeter data is given in Figure 9. The arrows represent the altimeter-derived annual mean transports between stations for upper-layer baroclinic transports (thick arrow) and for the geostrophic transport reference to 1000 m (thinner arrow).

Along 30S, both transports are either similar, or the geostrophic transport relative to 1000 m is larger than the transport of the upper layer. The latter is acceptable since the mean depth of the thermocline in the area is always less than 1000 m. The opposite is true for the sections farther south, indicating that either there is a strong flow in the opposite direction below the thermocline level, or that the two-layer model overestimates the transport, or both.

To investigate this situation, CTD data collected during the three BEST cruises are analyzed. For each CTD station, the depth of the 10°C isotherm, the dynamic height, the

Table 5. Comparison between the statistics of the transport series obtained by Garzoli *et al.* (1996) and the transports (14) calculated from the dynamic height series derived from the altimeter data.

Along 30S	Station pairs	Minimum	Maximum	Mean	Delta mean
Altimeter	62 and 2	2.9	8.3	4.7	
Moorings	*62 and 2*	*1.7*	*7.8*	*4.5*	*0.2*
Altimeter	2 and 3	−2.5	10.8	4.2	
Moorings	*2 and 3*	*−2*	*13.7*	*4.7*	*−0.5*
Altimeter	3 and 58	−2.5	8.3	1.1	
Moorings	*3 and 58*	*−6.1*	*5.6*	*0.4*	*0.7*
Altimeter	58 and 4	−7.2	14.1	3.8	
Moorings	*58 and 4*	*−4.9*	*15.1*	*5.3*	*−1.5*
Altimeter	4 and 61	−8.1	5.2	−1.6	
Moorings	*4 and 61*	*−15.5*	*7.8*	*−2.8*	*1.2*
Closed box	Station pairs	Minimum	Maximum	Mean	Delta mean
Altimeter	56 and 59	−5.3	17.8	2.7	
Moorings	*56 and 59*	*−7*	*19*	*4.1*	*−1.4*
Altimeter	56 and 62	−10.3	1.7	−3.2	
Moorings	*56 and 62*	*−10.4*	*0.9*	*−3*	*−0.2*
Altimeter	62 and 58	2.2	24	10.4	
Moorings	*62 and 58*	*1*	*20.3*	*9.6*	*0.8*
Altimeter	59 and 61	−7.6	13.6	5.1	
Moorings	*59 and 61*	*−11.5*	*18.6*	*4.2*	*0.9*
Altimeter	58 and 61	−5.5	11.7	3.1	
Moorings	*58 and 61*	*−2.7*	*11*	*3.6*	*−0.5*

value of g', the geostrophic velocities and transports, and the baroclinic transports from the two-layer model (10) are obtained. The analysis of the CTD data indicates that:

- Both transport estimates from the depth of the 10°C isotherm and dynamic height obtained from the altimeter data agree with the CTD data. This result is obtained by comparing the transports measured with the CTD data with the transports from the altimeter at that date (not shown).
- The two-layer model overestimates the surface flow in the southern section (Fig. 10a).
- Along 30S, the transports from the two-layer model are a good estimate of the upper layer transport (see Fig. 10b).

To complete this analysis, the transport from the two-layer model (12), the geostrophic transport obtained from the dynamic height as a function of depth, $T_r = \int V_g dz$, and the geostrophic transport calculated from the CTD data using the approximation applied to the IES data (16) (in Table 6, Approx. T_r), are presented in Table 6. All values are obtained from CTD data collected at the deployment sites during the three BEST cruises. The geostrophic transports from the dynamic height series of the surface relative to 1000 m, obtained by using approximation (16), are very similar to the geostrophic transports calculated for the same water column using the vertical information provided by the CTD data, $T_r = \int V_g dz$. The baroclinic transports calculated using the two-layer model formula-

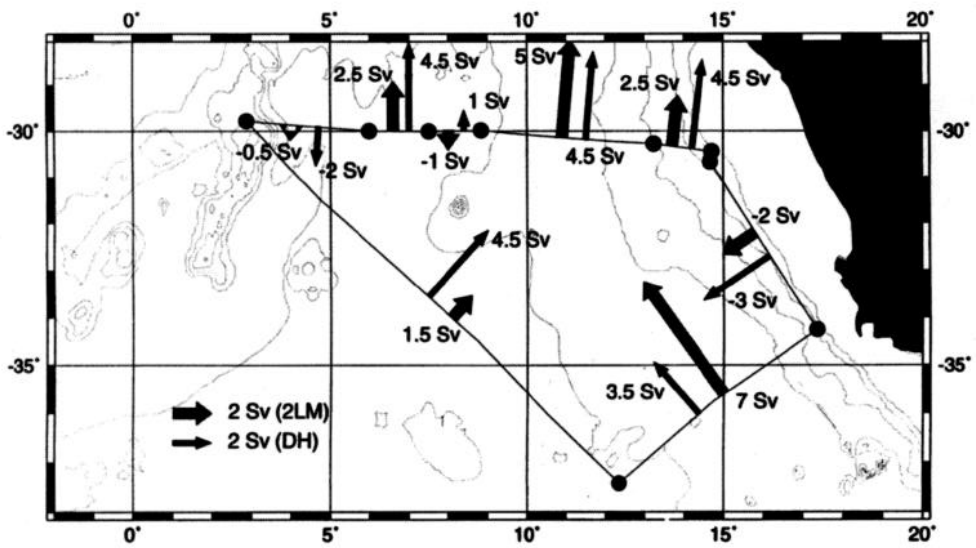

Figure 9. Comparison between the annual mean upper-layer baroclinic transport between stations obtained from the two-layer model (thick arrow) and from the geostrophic transports using the dynamic height series (thin arrow). Bathymetry is in 1000 m intervals.

tion, S_{cl}, are similar or smaller than the ones obtained with the CTD along 30S (station pairs 58–61 and 62–58). Farther south, between stations 59 and 56, the baroclinic transports from the two-layer model formulation are up to three times larger than the transports calculated from the CTD data.

4. Analysis of three years of data from the altimeter

Based on the encouraging results obtained in the previous section, the variability of the transports in the area over three-year long T/P series is now investigated. The time series are computed at the location of the moorings to compare them with values from the BEST data set in the early portion of the T/P mission. To increase the resolution of the BEST array, the same computations are done in regions of high variability located between IES 59 and 61, and 59 and 56, hereafter a through e (Fig. 1). The depth of the thermocline field is analyzed in Part 2 of this paper where the characteristics of the rings and the upwelling system are studied.

The three-year long dynamic height series of the surface relative to 1000 m are shown in Figures 11a,b. It is very interesting to note that along 30S (Fig. 11a), the previous results obtained by Garzoli and Gordon (1996) for the BEST period of observation are valid for the three years of the altimeter data. Elevations in dynamic height related to the passage of rings are observed at the western side of the section. The lowest values of dynamic height are observed close to the coast and might be related to the upwelling. The series of dynamic height as a function of latitude and time between sites IES 61 and IES 59 is shown in Figure 11b. The distribution of the highest values of dynamic height indicates that most of

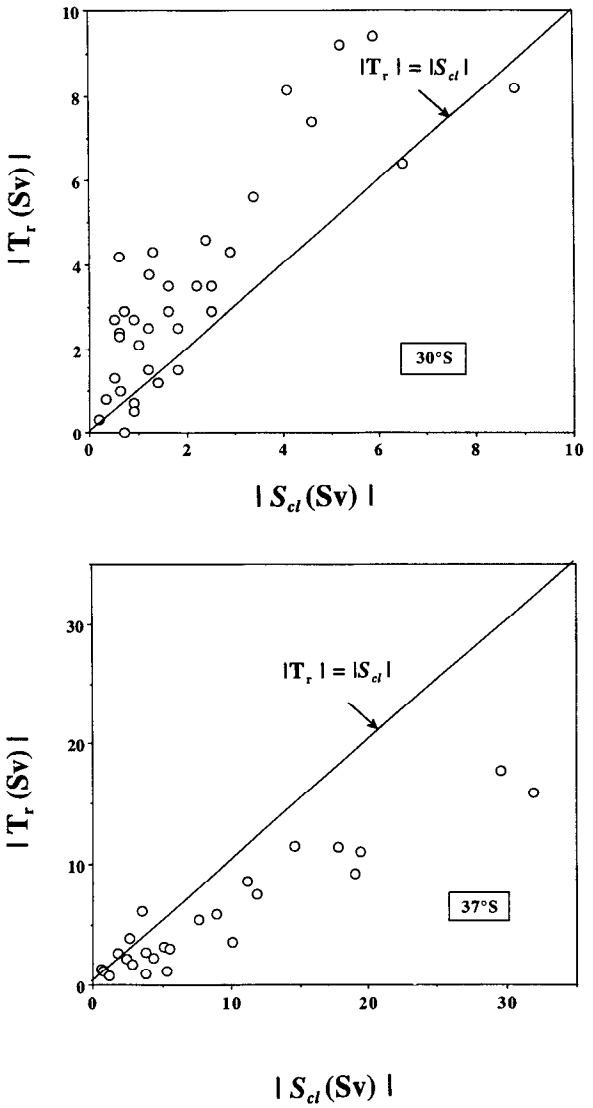

Figure 10. Relation between the absolute value of the geostrophic transport (surface to 1000 m) and the absolute value of the baroclinic component of the transport calculated from the two-layer model (surface to h_1). Values are obtained from the BEST CTD data using the g' obtained at each location: (a) between 36S and 37S; (b) along 30S. For both graphs the solid line represents when the absolute value of the two transports are equal.

the eddies crossed this section between 30S and 33S. Only twice, during mid 1994 and 1995, are eddies observed south of 34S. A more complete study of the eddies' trajectories will be done in the second part of this paper in which the eddy field is analyzed and discussed.

Table 6. Transports obtained from the CTD data collected during the three BEST cruises. $T_r = \int_0^{1000} v dz$; approx. T_r is the approximation given by (14) and S_{cl} are the baroclinic transports given by (10). In all cases results are from the CTD data.

BEST 1:

Station Pair	T_r(Sv)	Approx. T_r(Sv)	S_{cl}(Sv)
58–61	9.2	9.2	5.2
62–58	4.5	6	0.6
59–56	3.6	3.5	10.1

BEST 2:

Station Pair	T_r(Sv)	Approx. T_r(Sv)	S_{cl}(Sv)
58–61	−8.6	−5.9	−4.6
62–58	16.5	20.1	19
59–56	11.5	10.1	14.6

BEST 3:

Station Pair	T_r(Sv)	Approx. T_r(Sv)	S_{cl}(Sv)
58–61	8.2	8.1	4.1
62–58	4.3	6	2.9
59–56	5.4	4.1	7.6

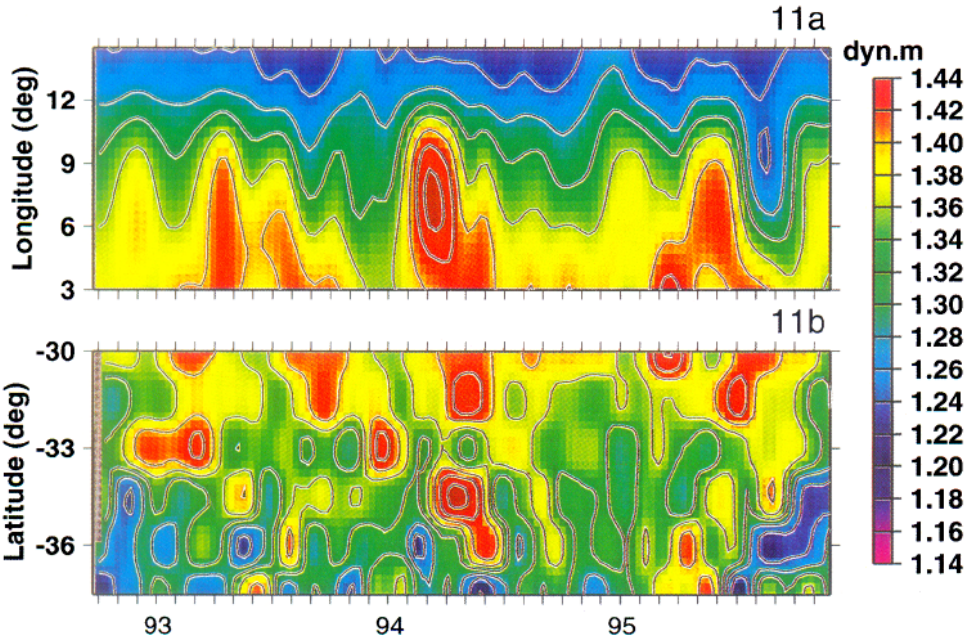

Figure 11. Time series of dynamic height of the surface relative to 1000 m obtained from the altimeter data at the locations indicated in Figure 1: (a) across 30S and (b) between stations IES 61 and IES 59. The red colors indicate the pressure of eddies, while the purple colors correspond to lower values of dynamic height.

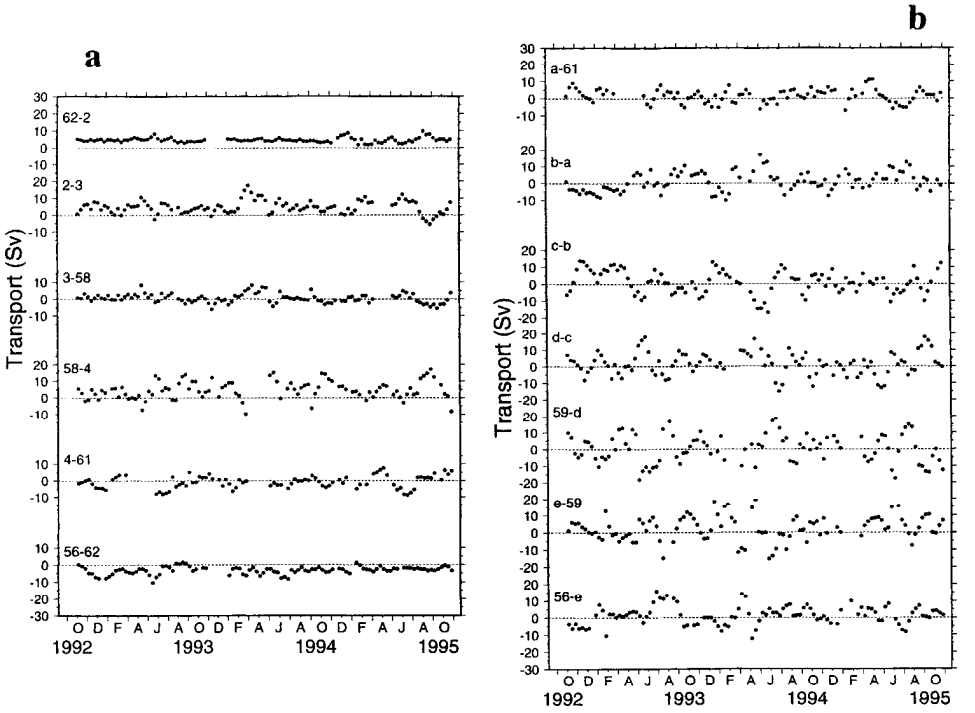

Figure 12. (a) and (b) Three-year series of the geostrophic transport (from the surface to 1000 m) obtained from the altimeter data between the mooring locations and at the interpolation points a, b, c, d, and e (Fig. 1).

The three-year long series of geostrophic transports of the upper kilometer in the region under analysis are given in Figures 12a,b. The transports are calculated from the dynamic height series following (16). The three-year mean of the series between each pair of sites is shown graphically in Figure 13.

Along 30S and east of 9E, where the steady component of the Benguela Current was previously observed (Garzoli and Gordon, 1996), the transport series indicates northward flow through the three years of observations (Fig. 12a) with just one reversal of the flow between stations 2 and 3 during August 1995. Closer to the African coast (between stations 62 and 2) the flow remains northward for the three observed years. The northward flow between 15E and 9E, based on a three-year mean, is 10 Sv. Maximum values of 15 to 20 Sv are observed between 9E and 14E (transports between stations 2 and 3, Fig. 11a) during March and April of 1993 and 1994. Unfortunately, no data was available from the altimeter during this period of time in 1995 to determine if this situation corresponds to a seasonal maximum. Farther west, between stations 58 and 3, the flow starts oscillating between positive and negative values with a net flow toward the north over the three years of less that 1 Sv. Between 7°30′E and the Walvis Ridge (3E), where the transient component of the Benguela Current is mostly confined, the transport oscillates between 20 Sv and

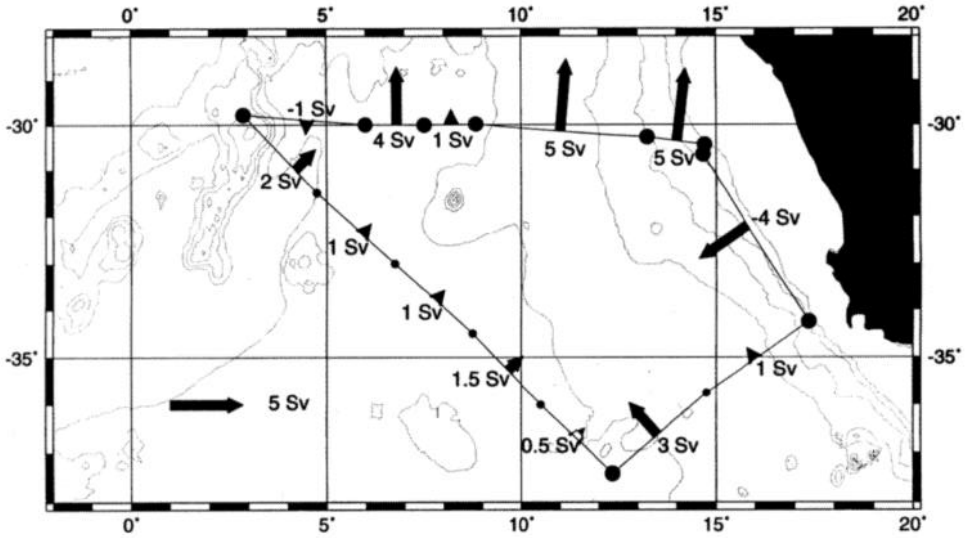

Figure 13. Calculated values of the three-year mean of the geostrophic transports between station pairs obtained from the altimeter data. Bathymetry as in Figure 1.

−10 Sv, with a net three-year mean of 3 Sv. This result indicates that the three-year mean transport of the Benguela Current across 30S between the instruments deployed at the African coast continental shelf and the Walvis Ridge is 14 Sv, within the limits of the computation errors. Of these 14 Sv, 6 Sv come (from geometry) from the South Atlantic, 3 Sv from the Indian Ocean, and 4 Sv from the east (Agulhas and tropical waters). Both the flow from the South Atlantic and the flow from the Indian Ocean exhibit large variability (Fig. 12a,b). The transport oscillates between +20 to −20 Sv, and these fluctuations are mostly related to the passage of rings. To illustrate these results, two cases are presented and discussed: July 8, 1993 and February 23, 1994. The geostrophic transports, the sea-height anomaly, and the sea-surface temperature are shown for each one of the two time periods mentioned above in Figures 14a through 14d.

The geostrophic transports for July 8, 1993 are indicated by arrows proportional to the transport magnitude and pointing in the direction of the flow in Figure 14a. Through the southern section of the box (between stations 59 and 56) 16 Sv enter the box and 15 Sv leave the box. The net flow between stations 56 and 59 is then 1 Sv. The sea-surface height (Fig. 14a) exhibits a region of high positive values, which indicates the presence of a ring crossing this section. In SST (Fig. 14b) the warm event appears as a field of advection of warm Indian Ocean water around the edge of the ring. Across the westernmost north-south section (between stations 61 and 59) the flow changes sign four times due to the presence of a warm ring in the southern side of the section and to an opposite circulation due to a depression on dynamic height in the northern side (arrows in Fig. 14a). This situation is confirmed by the sea-height anomaly picture (Fig. 14a) and in SST (Fig. 14b), due to the rapid loss of surface thermal signature of the Agulhas eddies as they migrate into the

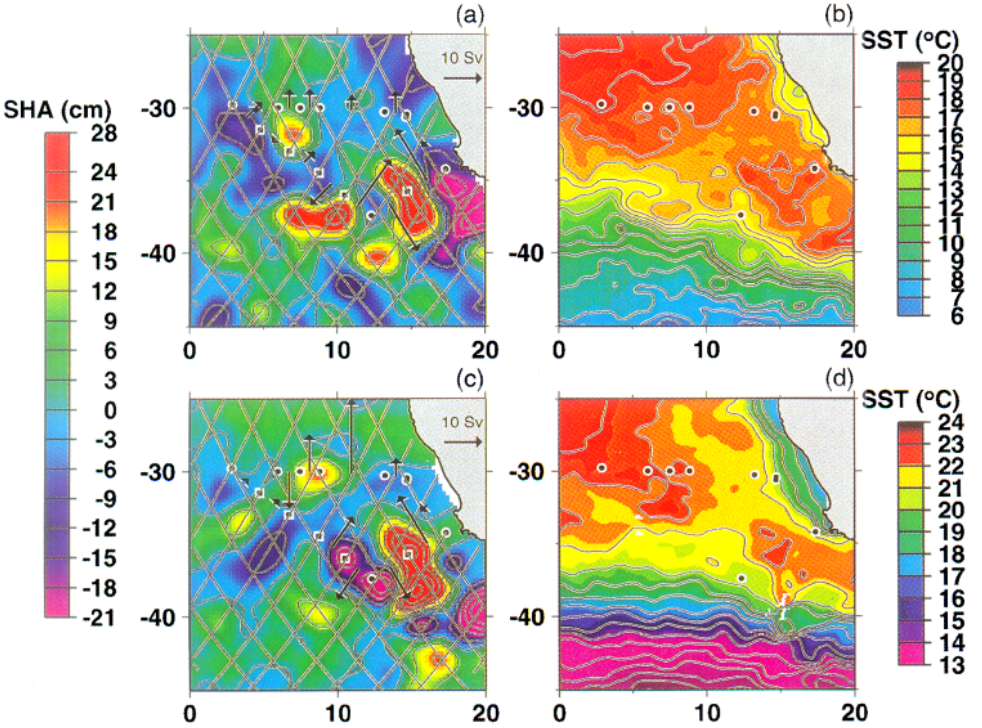

Figure 14. (a) Geostrophic transports from the surface to 1000 m in Sv (arrows) overlapped to sea-surface height for July 8, 1993; (b) Sea-surface temperature for July 8, 1993; (c) Same as (a) for February 23, 1994; (d) Same as (b) for February 23, 1994.

Atlantic. Along 30S, where the flow associated with the stationary part of the Benguela Current is confined east of 8E, another warm feature is observed approaching the easternmost stations (Fig. 14a). As a result, the flow between stations 61 and 4 is toward the south. The SST image shows a different picture where the scenario is similar but shifted in surface toward the east. This could be an indication that the SST representation of the currents and eddy field in the region are not coincident with the deep or integrated expression of the same field. Similar shifts have been observed in the Brazil/Malvinas confluence region (Garzoli and Garraffo, 1989; Goñi *et al.,* 1996).

On February 23, 1994 (Figs. 14c,d), the geostrophic transports, the SST image, and the surface height anomaly fields suggest a ring presumably from the Agulhas retroflection between stations 59 and 56. The transports (Fig. 14c) indicate a rotational circulation, with 15 Sv entering and 10 Sv leaving the area. A higher value of sea-surface height anomaly is evident at this location (Fig. 14c) which is associated with an increase in the SST (Fig. 14d). On the southern edge of the north-south section (stations 61 to 59) the transport estimates indicate a clockwise rotation (Fig. 14c). The map of sea height anomaly (Fig. 14c) indicates a low in dynamic height, and the SST image (Fig. 15d) shows colder

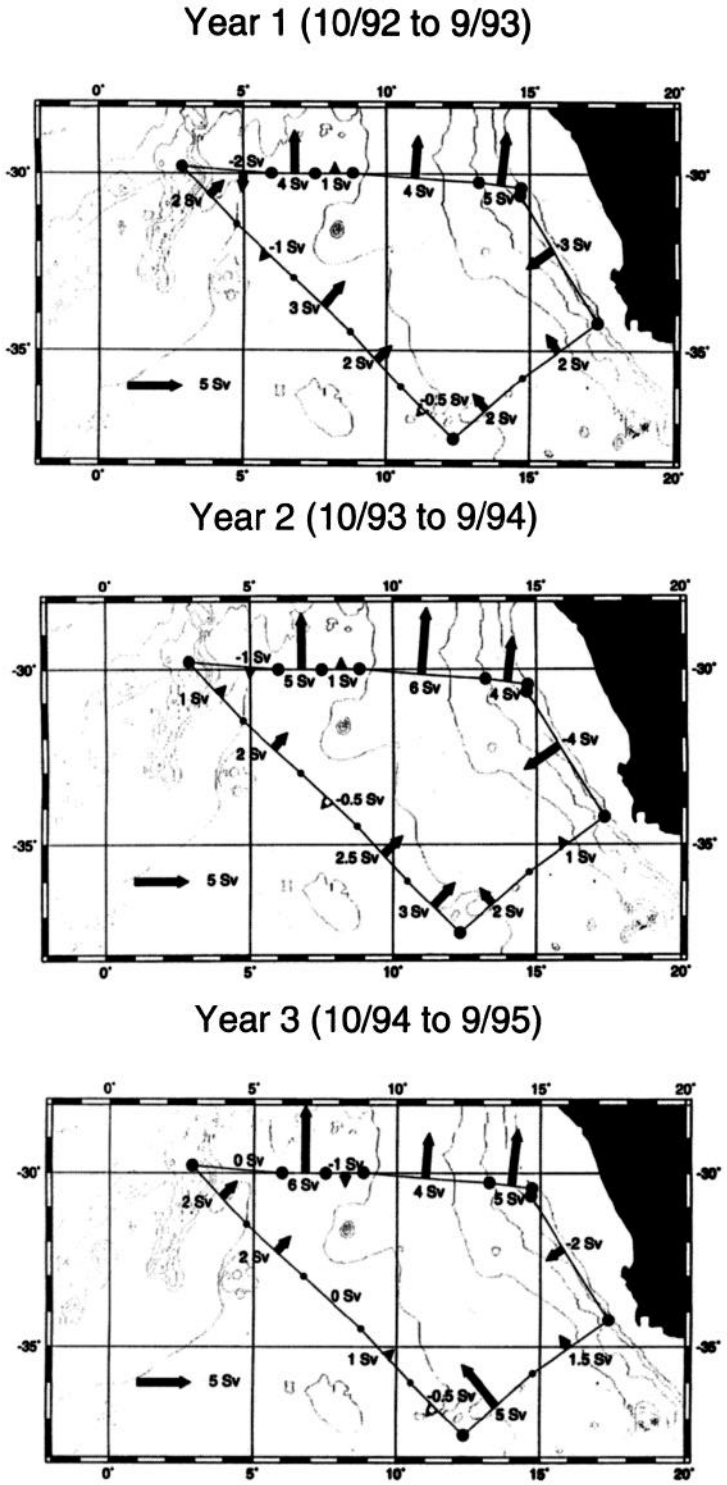

Figure 15. Mean transports from the surface to 1000 m for: (a) Year 1: October 1992 to September 1993; (b) Year 2: October 1993 to September 1994; and (c) Year 3: October 1994 to September 1995. Bathymetry as in Figure 1.

Table 7. Different components of the Benguela Current analyzed per year and for a three-year mean.

	Year 1	Year 2	Year 3	3-Year Mean
Total Transport	12 Sv	15 Sv	14 Sv	14 Sv
From the South	50%	53%	36%	44%
From the Indian	33%	20%	50%	28%
From the East	25%	27%	14%	28%

temperatures at this site, suggesting a cyclonic eddy. A warm ring is observed also along 30S as higher values of η' are practically centered between stations 3 and 58. The associated upper kilometer transports are symmetric 10 Sv toward the north and 10 Sv toward the south.

a. Seasonal and interannual variability. The altimeter data offer the possibility to analyze annual features in the transport fluctuations. Results are shown in Figure 15 and Table 7. In a previous section, the three-year mean transports were analyzed and it was determined (Fig. 13) that of the 14 Sv that the Benguela Current transported north into the South Atlantic across 30S, 28% came from the tropics (4 Sv), 28% from the Agulhas retroflection (4 Sv), and 44% from the South Atlantic (5 Sv). During Year 1 (October 1992 to September 1993), the mean Benguela Current transport across 30S is 12 Sv (Table 7), in agreement with the results obtained from the IES data (Table 5). For Years 2 and 3, the mean transport across 30S is 15 Sv and 14 Sv, respectively (Table 7). These three means are within the limits of the errors, basically similar. Therefore, it can be concluded that the Benguela transport into the Atlantic across 30S is between 12 Sv and 15 Sv and that this transport does not vary significantly from one year to the other. Variations are observed on the sources from where the Benguela Current drains its components. The way these different sources vary is shown schematically in Figure 15 and summarized in Table 7. During Years 1 and 2, the major contribution to the Benguela Current is from the South Atlantic (50%), while in Year 3, 50% of the volume is drained from the Indian Ocean. Apparently the reason why the higher value is observed during Year 2 is because more water was drawn from the east. That is to say, a stronger Benguela coastal current drains more water from the tropics.

Analysis of the periodograms indicates that there is an annual peak in the dynamic height series along 30S, from 15E to 6E (Fig. 16) of the geostrophic transports. While the annual peak is significant at all locations along 30S and east of 3E (not shown), it is not present at station 61, located at the Walvis Ridge. The same is valid at station 56 (not shown), located at the edge of the continental shelf. This appears as an indication that large topographic effects influence the periodicity. At station 59, the dominant peak is at 220 days and might be related to the eddy field. A similar periodicity (230 days) was observed in the eastern basin of the North Atlantic from TOPEX data (Rogel *et al.,* 1995). Synoptic maps show that this westward propagating feature corresponds to eddies and rings.

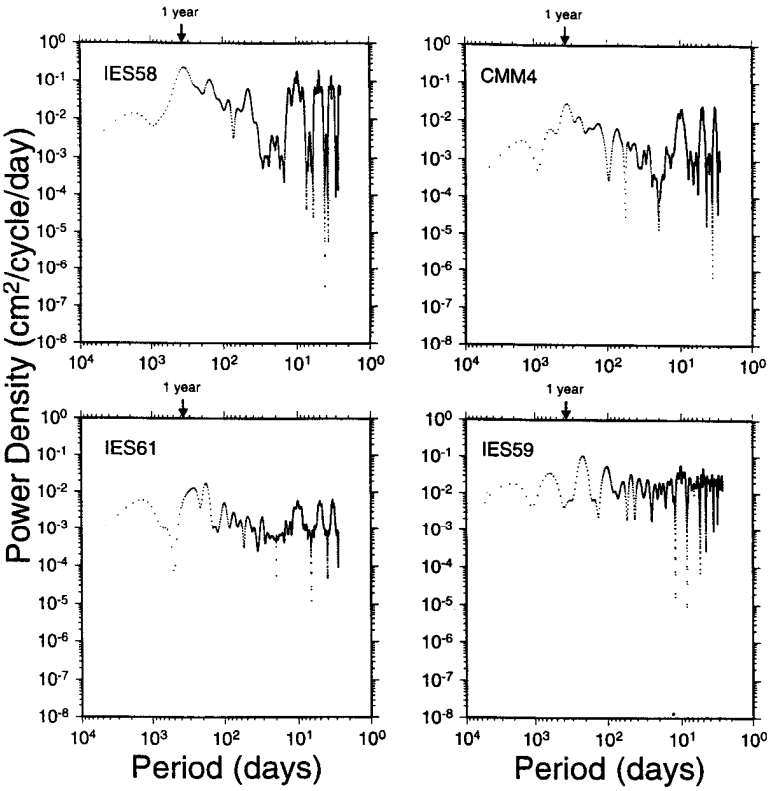

Figure 16. Examples of periodograms at sites IES 58, CMM2, IES 61, and IES 59. A one-year period is visible in IES 58 and CMM4.

b. The barotropic transport. The Benguela Current has a large barotropic component due to the eddy field (see Chassignet *et al.*, 1989). Garzoli *et al.* (1995) determined that for the steady part of the Benguela Current the barotropic transport was 25% of the total flow, while in the transient part, and due to the barotropic characteristic of the eddy field, the barotropic flow was 75% of the total flow. In this section, these results are used to determine the validity of the model applied to calculate the barotropic component of the flow (Goñi *et al.*, 1996). The procedure is as follows.

The upper-layer total transport from the two-layer model is given by

$$S_T(t) = \frac{g}{f}\overline{h_1}(t)\Delta\eta(t). \tag{18}$$

where $\overline{h_1}(t)$ is the mean upper-layer thickness between pairs of stations. A value for the barotropic transport can be obtained knowing the total transport and the baroclinic transport. In Section 3 we showed that the two-layer model approximation is best along 30S. Therefore, (18) is applied only for the stations along this latitude. The barotropic transports are calculated for station pairs 61 and 58, and 58 and 62, and compared with the

results obtained from the pressure gauges by Garzoli *et al.* (1996) at the same locations. Through the combination of IES and pressure sensors, Garzoli *et al.* (1996) determined that in the upper 2600 m of the water column the components of the flow were as follows:
Between stations (62–58) (transient component): $S_{cl} = 3$ Sv and $S_{tr} = -11$ Sv;
Between stations (58–61) (steady component): $S_{cl} = 10$ Sv and $S_{tr} = -11$ Sv.

The upper-layer total transport between pairs of stations is estimated using the sea height anomalies and varying the mean sea level differences between −0.15 to 0.15 m. The mean sea heights that balance the total upper layer transports are averaged and taken as the estimated sea height difference between pairs of stations. The estimated mean sea level difference from the altimeter data is 0.01 m between stations 61 and 58 and 0.08 m between stations 58 and 62.

Using the estimated values of $\Delta\eta$, the total transports obtained from (18) are: $S_T(61\text{–}58) = 0.6$ Sv and $S_T(58\text{–}62) = 3.5$ Sv. These totals are the sum of the barotropic and the baroclinic components (i.e., $S_{cl} + S_{tr}$). Therefore, using the previously computed values for the upper-layer baroclinic transports between these two stations pairs, which are $S_{cl}(61\text{–}58) = 2.3$ Sv and $S_{cl}(58\text{–}62) = 5.2$ Sv, the upper layer barotropic transports (from the surface to the depth h_1) are: $S_{tr}(61\text{–}58) = -1.7$; $S_{tr}(58\text{–}62) = -1.7$. Therefore, the barotropic component of the total flow is of the same order of magnitude (~ -2 Sv) in the upper layer ($z < h_1$) for both the transient and steady parts of the Benguela Current. Similarly, the contribution of the baroclinic flow in the transient part of the Benguela Current is half of the one in the steady part.

To complete this analysis the baroclinic transport results are compared with those previously obtained by Garzoli *et al.* (1996) using the relation,

$$S_{tr} = V_P h \Delta x, \tag{19}$$

where h is 2600 m and V_P is the geostrophic velocity between station pairs obtained from the pressure measurements. If, for the effect of the comparison, h is replaced by the mean depth of the thermocline, $h_{1,(61\text{–}58)} = 410$ m, and $h_{1,(58\text{–}62)} = 323$ m, the values obtained for the barotropic transports are

$$S_{tr}(61\text{-}58) = -1.6 \text{ Sv} \qquad S_{tr}(58\text{-}62) = -1.4 \text{ Sv},$$

Therefore, the two-layer model along 30S reproduces in orders of magnitude, the same results obtained from a combination of IES and pressure sensors.

5. Summary and conclusions

The most important result of this paper is the demonstration that, in combination with *in-situ* data, the altimeter data can be used to reliably monitor the transports in the southeastern South Atlantic. The comparison between altimeter data and moored instruments proved that the sea-surface elevation anomaly is directly correlated to the depth of the thermocline and to the surface dynamic height. Knowing these correlations, it is possible to calculate the transports by using a two-layer model or a linear stratification geostrophic relation. In this particular region, the analysis performed in this paper indicates

that transports obtained from the two-layer model are overestimated on the southern limb of the gyre. This is more pronounced in the region of the Agulhas retroflection where the values obtained are more than double the values obtained from moored instrumentation. These differences are smaller in the region of the Benguela Current but still the transports of the upper layer, from the surface to the depth of the 10°C isotherm, are equal or smaller than the geostrophic transports from the surface to the upper kilometer. Considering that the main depth of the thermocline in this region is always less than 1000 m, this is an indication that, by a lesser amount, the Benguela transports calculated by this method are still overestimated.

If the geostrophic relation is applied to the dynamic height series derived from the sea-surface height, the transports obtained are similar to the ones calculated with the moored instruments. These results indicate that in this region more than two layers might be needed to model the oceanic vertical structure, and that a better estimate for the transports is obtained by scaling the sea-surface height elevation to surface dynamic height. In the region where the two-layer model more accurately describes the upper layer transport, the model can be successfully used to calculate the total and barotropic transports of the Benguela Current.

The analysis of the three years of geostrophic transport obtained from the altimeter data indicates that the Benguela Current transport does not undergo a remarkable interannual variability. Changes are observed on smaller scales due to the high variability of the region, in particular when rings are detached from the main flow and migrate into the Atlantic. In the mean, the baroclinic northward transport ranges between 12 and 15 Sv, with fluctuations that reach up to 25 Sv due to the high velocities associated with the rings' shear. Even though the main transport is very steady, the source waters of the Benguela Current changes from year to year. In the mean, the main contribution comes from the South Atlantic and the contributions from the Indian Ocean and the tropical Atlantic are equally partitioned. However, the analysis of the three years indicates that this is only the case during 1993 and 1994. During 1995, the main contribution is from the Indian Ocean. The reasons for these changes cannot be determined from the present analysis. Nonetheless, we can speculate that the wind may play an important role in determining how much water is drained from the coastal area of tropical Atlantic origin or from the South Atlantic by changing the intensity and/or location of the gyre.

Acknowledgments. Support for collection and reduction of the BEST data sets was provided by NSF grants OCE91-02722 and 94-01950. The SST images under N00074-89-J1144 and NOAA/ University of California; and the altimeter data under N00014-89-10166. A. Roubicek produced the computer-generated figures; J. Carpenter collaborated with the final version of some of the graphics; G. Derr prepared the manuscript for submission; and E. Ryan generated the objective analysis of the sea-surface temperature field.

REFERENCES

Cartwright, D. E. and R. D. Ray. 1990. Oceanic tides from Geosat altimetry. J. Geophys. Res., *5,* 3069–3090.

Chassignet, E. P., D. B. Olson and D. B. Boudra. 1989. Evolution of rings in numerical models and observations, *in* Mesoscale Coherent Structures in Geophysical Turbulence, Proceedings, 20th International Liege Colloquium on Ocean Hydrodynamics, 337–356.

Chelton, D. B., M. G. Schlax, D. L. Witter and J. G. Richman. 1990. GEOSAT altimeter observations of the surface circulation of the Southern Ocean. J. Geophys. Res., *95,* 17,877–17,903.

Cheney, R. E., B. C. Douglas, R. W. Agreen, L. Miller, D. L. Porter and N. S. Doylem. 1987. GEOSAT altimeter geophysical data record user handbook. NOAA Tech. Memo., NOS NGS-46, 32 pp.

Chiswell, S. M., D. R. Watts and M. Wimbush. 1986. Using inverted echo sounders to measure dynamic height in the eastern equatorial Pacific during the 1982–1983 El Niño. Deep-Sea Res., *33,* 981–991.

Duncombe-Rae, C. M., S. L. Garzoli and A. L. Gordon. 1996. The eddy field of the southeast Atlantic Ocean: A statistical census from the BEST project. J. Geophys. Res.-Oceans, *101,* (C5), 11,949–11,964.

Garzoli, S. L. and Z. Garraffo. 1989. Transports, frontal motions, and eddies at the Brazil-Malvinas Currents confluence. Deep-Sea Res., *36,* 681–703.

Garzoli, S. L. and A. L. Gordon. 1996. Origins and variability of the Benguela Current. J. Geophys. Res.-Oceans, *101* (C1), 897–906.

Garzoli, S. L., A. L. Gordon and C. M. Duncombe-Rae. 1995. Benguela Current sources and transports. U.S. WOCE Rept., 17–19.

Garzoli, S. L., A. L. Gordon, V. Kamenkovich, S. Pillsbury and C. M. Duncombe-Rae. 1996. Variability and sources of the southeastern Atlantic circulation. J. Mar. Res., *54,* 1039–1071.

Goñi, G., S. Kamholz, S. L. Garzoli and D. Olson. 1996. Dynamics of the Brazil/Malvinas confluence based on inverted echo sounders and altimetry. J. Geophys. Res.-Oceans, *101* (C7), 16,273–16,289.

Gordon, A. L. 1985. Indian Atlantic transfer of thermocline water at the Agulhas retroflection. Science, *222,* 1030–1033.

Hayne, G. S., D. W. Hancock, III and C. L. Purdy. 1994. The corrections for significant wave height and attitude effects in the TOPEX radar altimeter. J. Geophys. Res., *99* (C12), 24,941–24,955.

Katz, E. and S. L. Garzoli. 1982. Response of the western equatorial Atlantic Ocean to an annual wind cycle. J. Mar. Res., *40,* (Suppl.), 307–327.

Lutjeharms, J. R. E. and R. C. van Ballegoyen. 1988. The Agulhas Current retroflection. J. Phys. Oceanogr., *18,* 1570–1583.

Mariano, A. J. and O. B. Brown. 1992. Efficient objective analysis of dynamically heterogeneous and nonstationary fields via the parameter matrix. Deep-Sea Res., *39* (7–8A), 1255–1271.

Olson, D. B. and R. H. Evans. 1986. Rings of the Agulhas Current. Deep-Sea Res., *33* (1A), 27–42.

Peterson, R. G. and L. Stramma. 1991. Upper-level circulation in the South Atlantic Ocean. Prog. Oceanogr., *26,* 1–73.

Rogel, P., J. F. Minster, E. Blayo, J. M. Molines and J. Verron. 1995. Observation and assimilation of propagating Rossby waves in the North Atlantic Ocean. EOS, Trans., Amer. Geophys. Un., *76,* 46.

Stramma, L. and R. G. Peterson. 1990. The South Atlantic Current. J. Phys. Oceanogr., *20,* 846–859.

Watts, R. and T. Rossby. 1977. Measuring dynamic heights with inverted echo sounders: Results from MODE. J. Phys. Oceanogr., *7,* 345–358.

Received: *20 August, 1996;* revised: *2 December, 1996.*